Forced Wetting and Hydrodynamic Assist

Terence D. Blake,* Guillaume Doyen, Juan-Carlos Fernandez-Toledano,
and Joël De Coninck
Laboratory of Surface and Interfacial Physics
University of Mons, 7000 Mons, Belgium

* **E-mail**: terrydblake@btinternet.com

Abstract

Air entrainment sets the ultimate limit to coating speeds. However, it is well known that it can be postponed to higher line speeds by manipulating the coating flow to generate 'hydrodynamic assist.' Experiments have shown that the conditions that produce higher coating speeds also reduce the apparent dynamic contact angle, suggesting a direct link, but the mechanism by which the flow might affect wetting speeds and the dynamic angle is unclear. Here we develop an earlier proposal that an intense shear stress in the vicinity of the moving contact line can assist surface tension forces in compensating for contact-line friction. This reduces the velocity-dependence of the contact angle and so postpones air entrainment. Viewed in this way, hydrodynamic assist is simply a natural consequence of forced wetting that emerges when the contact line is driven by a strong and highly confined flow capable of inducing slip between the liquid and the solid. We present the results of large-scale molecular dynamics simulations of forced wetting in support of these ideas and use the molecular-kinetic theory of dynamic wetting to place them on a quantitative footing.

Introduction

To successfully coat a liquid onto a solid, the liquid must wet the solid to a sufficient degree, else it will retract from the surface. The final adhesion will also be poor. The degree of wetting is characterized by the contact angle θ, i.e. the angle subtended by the surface of the liquid at the three-phase contact line where liquid, solid and the external phase (usually air) all meet. The contact angle at equilibrium θ^0 depends on the relative strength of liquid-liquid and solid-liquid interactions. Smaller angles indicate more complete wetting and better adhesion. However, the instantaneous value of the angle also depends on the rate of wetting, with advancing angles increasing and receding angles decreasing with the speed U_{CL} at which the contact line moves across the solid surface. At sufficiently high rates of wetting the dynamic contact angle θ_D approaches its limiting value of 180° and air is entrained. This sets the ultimate limit to line coating speeds. In consequence, if we wish to model coating we must first be able to model dynamic wetting and predict its limits. As a further complication, it is known that air entrainment can be postponed to higher line speeds by manipulating coating flows to generate what has been termed 'hydrodynamic assist' [1]. The technique is well established in the coating art, but the mechanism by which it works is unclear, although there is an increasing consensus that it depends on controlling liquid flow in the vicinity of the contact line through some form of geometric or hydrodynamic confinement [1–4]. It is this topic that we address in our paper.

Models of dynamic wetting

Despite much study, the mechanism of dynamic wetting has been the source of controversy for at least 50 years and is still not fully resolved. There are three main theories [5]. One idea is that the behavior of the dynamic contact angle is due to hydrodynamic (viscous) bending of the liquid/air interface, at a scale below that at which the angle is measured, but larger than the molecular scale at which hydrodynamics is normally thought to break down [6,7]. At this molecular scale it is usually assumed that the local angle retains its equilibrium value. In a significant variant of this model (the interface-formation model), the variation in the dynamic angle is due mainly to changes in the local surface tensions of the various interfaces meeting at the moving contact line. These changes are caused by the need to create or destroy new solid-liquid interface at a finite rate. A key assumption is that the

relaxation times of the surface tensions are sufficiently long as to generate local surface tension gradients, which interact with the flow [8]. The third idea, and the first suggested, is that the dynamic contact angle is due to a local frictional force operating directly at the contact line. The friction is due to the interaction of the liquid molecules at the advancing front with the potential-energy landscape of the solid surface and is therefore closely related to ideas of molecular slip at a solid-liquid interface. The friction is opposed by the out-of-balance surface tension force $\gamma_L(\cos\theta^0 - \cos\theta_D)$, where γ_L is the surface tension of the liquid. This model is usually known as the molecular-kinetic theory (MKT) [9,10].

All three theories have their limitations. The standard hydrodynamic model is based on lubrication methods and predicts a singularity at the moving contact line as a result of the conflict between a contact line that moves and the usual no slip boundary condition. The problem is overcome by allowing slip in the vicinity of the contact line, but the resulting kinematics, with a stagnation point on the liquid-air interface, appear to conflict with experiment [8]. The interface-formation model has been criticized on the grounds that surface tensions relax on a time-scale that is too fast to generate local gradients that could interact with the flow. While this seems to be true for simple liquids [11], it is not necessarily the case for complex ones, such as those containing surfactants. Finally, while the MKT does account quite realistically for the influence of liquid viscosity η_L and solid-liquid interactions, as characterized by the work of adhesion $Wa^0 = \gamma_L(1+\cos\theta^0)$ [12], it lacks any direct link to the hydrodynamics and can therefore provide only a boundary condition to the flow.

All the models account for much of the observed behavior, yet none is fully predictive: each requires some degree of curve fitting to extract key parameters. Thus, it has proved impossible to determine by direct experiment, which, if any, of the above models is nearer to the truth. Since more than one mechanism could operate, combined models have been proposed, involving both viscous bending and contact-line friction, but it has proved equally difficult to attribute the contribution of each mechanism. Because of this uncertainty, much recent effort to understand dynamic wetting has been devoted to non-experimental methods, using techniques such as lattice-Boltzmann simulations [13], molecular dynamics (MD) based on Lennard-Jones interactions [e.g. 14–17], diffuse interface models [e.g. 18,19] and hybrid schemes [e.g. 20]. Considerable progress has been made.

The results obtained using MD appear particularly telling. Due to computational limitations, current MD simulations are necessarily restricted to small systems (< 1μm) and short timescales (< 1 ns). Nevertheless, realistic behavior is observed. For example, thermodynamic relationships such as Young's equation for the equilibrium contact angle, the Laplace equation for the pressure drop across an interface and Poiseuille flow have all been verified. The capillary numbers $Ca = \eta_L U/\gamma_L$ observed in simulations of wetting are also in accord with experiment ($0 < Ca < 1$). In particular, simulations of spreading drops [15–17] have revealed that the local contact angle is indeed velocity-dependent, as predicted by the contact-line friction model, with no direct evidence of viscous bending. Furthermore, it has been shown that the values of parameters obtained by fitting the spreading data to the MKT are in close agreement with those found by directly interrogating the molecular dynamics [15,17]. Forced wetting has also been studied using MD with similar results [21]. Very recently [11], clear evidence has been found of a tangential force acting on the liquid from the solid substrate directly at the contact line and sufficient to account for the change in the contact angle from its equilibrium to its dynamic value. This force acts over a distance commensurate with interfacial thickness and so would be modeled at hydrodynamic length scales as a Dirac delta function. Thus, contact-line friction would appear to be a real phenomenon. It is no longer sufficient to assume that the local angle is unchanged.

What implications do these findings have for hydrodynamic assist? The question may be illustrated with reference to curtain coating. Experiments [1,22,23] show that air-entrainment can be postponed to speeds that are several multiples of those found in simple dip coating. This is achieved by adjusting the curtain flow rate and impingement angle so as to position the contact-line immediately beneath the foot of the curtain. Direct visualization experiments [22,24] have revealed that the associated dynamic

contact angle measured at the 10 μm scale is significantly flow dependent, with the smallest angles occurring under the same conditions as those that optimally postpone air entrainment. The obvious interpretation is that the two phenomenon are linked in some way.

Just how the flow might affect the dynamic contact angle is an open question. It has been argued [22] that for this to happen, some aspects of the physics responsible for the dynamic contact angle must be on the scale of the flow, i.e. non-local to the contact line. The original proposal was that this physics had its origin in the surface tension gradients that are central to the interface-formation model. But if these are called into question then this mechanism fails as a general explanation – though some consolation can be drawn from the fact that so far all the experimental evidence for hydrodynamic assist has been obtained with solutions rather than simple liquids. Finite element simulations of coating flows, based on the assumption of a fixed microscopic angle and slip near the contact line, suggest that the observed reduction in the dynamic contact angle on experimental length scales could be due to a confined flow close to the contact line giving better control of the pressure field generated in the displaced air as the dynamic angle increases, forcing the air into an ever narrowing wedge [4]. Ultimately, the presence of the air must be relevant to air-entrainment.

On the other hand, if the dynamic contact angle is due mainly to contact-line friction rather than viscous bending, as the MD evidence now suggests, then hydrodynamics must have some way of influencing it at the same molecular scale, otherwise air-entrainment would automatically ensue once the friction had driven the angle to 180˚. While a gradual thickening of the entrained air from a molecular layer to a visible one cannot be ruled out, it does not seem to be the norm, as the onset of air-entrainment is usually sudden and catastrophic. Therefore, a smooth transition at an angle of 180˚ to some sort of lamination process seems unlikely to provide a general explanation for the observed delay in wetting failure, except, perhaps, for extremely viscous liquids. One way in which hydrodynamics might have an effect on the dynamic contact angle at the molecular level has already been outlined within the framework of the MKT [10]. The essential idea is that if the shear field in the vicinity of the contact line is sufficiently intense and appropriately directed then it might assist the out-of-balance surface tension force in overcoming contact-line friction. The net result would be a reduction in the dynamic contact angle and the postponement of air entrainment.

It is this idea that we explore below, using large-scale molecular dynamics to compare both forced and spontaneous wetting for the same systems within the general framework of the MKT. As far as we are aware, this is the first time that MD has been used to make such a direct comparison. In addition, because MD systems are inherently small, any effect of confinement should be very clear. By spontaneous wetting, we mean that which occurs when a liquid drop is placed on a solid surface and spreads towards its equilibrium configuration. During this process, the contact angle relaxes, from 180˚ at contact, towards its equilibrium value θ^0. By forced wetting, we mean any method by which the contact line is driven across the solid surface at a steady rate at some dynamic contact angle $\theta_D > \theta^0$, as in liquid coating. Equilibrium is not attained and progress towards it is frustrated by the steady displacement. It is usually assumed that both processes have the same underlying mechanism, whatever it might be, but as we will show, the resulting dynamics can be quite different. What emerges is that hydrodynamic assist may be a specific, beneficial consequence of forced wetting in confined systems. While this has been suspected for some time, there has been no direct evidence.

The molecular-kinetic theory (MKT)

The model has been described extensively in previous publications, so a brief summary is sufficient for present purposes. First proposed over 40 years ago by Blake and Haynes [9], the model was later extended to include the specific effects of liquid viscosity [10] and solid-liquid interactions [25]. Insight gained through MD studies has refined some details and the model continues to evolve. There are two key parameters κ^0, the equilibrium frequency of random molecular displacements (jumps) of the liquid molecules at the surface of the solid, and λ, the average distance of each jump. The frequency κ^0 is

governed by the thermal activity of the molecules within the energy landscape of the solid, pictured as an array of potential energy wells where the molecules reside briefly between jumps – i.e. adsorption sites. The spatial distribution of these sites governs λ. The principal equation relating the speed of the contact line to the dynamic contact angle is

$$U_{CL} = 2\kappa^0 \lambda \sinh\left[\gamma_L\left(\cos\theta^0 - \cos\theta_D\right)\Big/ 2nk_BT\right] \tag{1}$$

where n is the number of adsorption sites per unit area, k_B is the Boltzmann constant and T the absolute temperature. At equilibrium, $\theta_D = \theta^0$, the surface tension driving force is zero and the contact line merely fluctuates about some mean position. When equilibrium is disturbed, the contact angle deviates from its equilibrium value and the resulting out-of-balance surface tension force $\gamma_L(\cos\theta^0 - \cos\theta_D)$ drives the system towards equilibrium against the friction caused by the drag of the solid on the molecules at the moving contact line. Assuming the adsorption sites to be uniformly distributed and that jumps occur between adjacent sites, $n \approx 1/\lambda^2$. If the argument of the sinh function in (1) is small (e.g. for liquids of low surface tension or near θ^0) then (1) reduces to a linear condition:

$$U_{CL} = \kappa^0 \lambda \gamma_L\left(\cos\theta^0 - \cos\theta_D\right)\Big/ nk_BT = \gamma_L\left(\cos\theta^0 - \cos\theta_D\right)\Big/ \zeta \tag{2}$$

where $\zeta = nk_BT/\kappa^0\lambda \approx k_BT/\kappa^0\lambda^3$ is the coefficient of contact line friction (per unit length of the contact line). It has been proposed [25] that κ^0 can be related to η_L and Wa^0 by

$$\kappa^0 = \left(k_BT/\eta_L v_L\right)\exp\left(-Wa^0/nk_BT\right) \tag{3}$$

This leads to

$$\zeta = \left(n\eta_L v_L/\lambda\right)\exp\left(Wa^0/nk_BT\right) \tag{4}$$

There is good evidence to support this proposal from both experiment and MD [e.g. 12,17,25,26].

In general, κ^0 and λ are obtained from by fitting eq. (1) to dynamic contact angle data. The values found from experiment are consistent with the model; thus, λ is of the order of molecular dimensions and while κ^0 can vary by many orders of magnitude, it increases steadily with both viscosity and solid-liquid interaction. In the MD simulations, the values can be obtained both by curve fitting and directly from the computations. Good agreement is found [15,17].

Molecular dynamics simulations of forced wetting

We have previously carried out large-scale MD simulations of liquid drops spreading under the action of surface tension alone [15,17]. In such cases, the velocity of the contact line continually decreases towards zero as the contact angle relaxes towards its equilibrium value.

Here, we consider wetting in which the contact line is forced to move at a fixed rate, which is then varied systematically to investigate the change in the contact angle with contact-line speed. Couette type flow is studied. A liquid bridge is positioned between two parallel planar solid plates that are moved at equal speeds in opposite directions, as illustrated schematically in Figure 1.

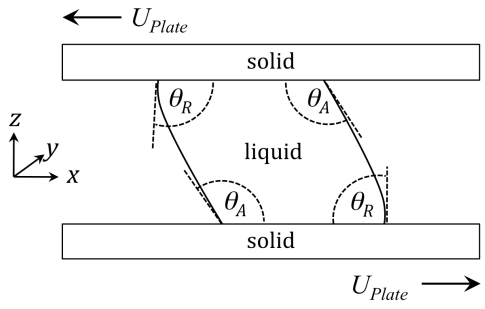

Fig. 1: System used for forced wetting simulations, showing advancing and receding dynamic contact angles, θ_A and θ_R.

To allow a strict comparison with the results obtained from our drop spreading simulations, the same methods, base

parameters and potentials are used. These have been detailed in previous publications [e.g. 17]. Briefly, we model the liquids, the solids and their interactions using Lennard-Jones potentials:

$$V_{ij} = 4C_{A-B}\varepsilon_{ij}\left[\left(\sigma_{ij}/r_{ij}\right)^{12} - \left(\sigma_{ij}/r_{ij}\right)^{6}\right] \quad (5)$$

where r_{ij} is the distance between any pair of atoms i and j. The coupling parameter C_{A-B} enables us to tune the relative affinities between the different types of atoms: solid-solid (*S*-*S*), liquid-liquid (*L*-*L*) and liquid-solid (*L*-*S*). The parameters ε_{ij} and σ_{ij} are related, respectively, to the depth of the potential wells and an effective atomic diameter. For both solid and liquid atoms ε_{ij} = 33.33 K (4.6×10^{-22} J) and σ_{ij} = 0.35 nm. The pair potential is set to zero for $r_{ij} = 2.5\,\sigma_{ij}$. C_{A-B}, is given the value 1.0 for both the *L*-*L* and *S*-*S* interactions, but for the *L*-*S* interaction it is varied between 0.4 and 0.8 to explore a range of equilibrium contact angles (136˚ to 75˚). The masses of all the atoms are equated to that of carbon. As before [17], all the simulations are carried out at a temperature of 33.33 K, kept constant using a thermostat based on velocity scaling and applied separately to the liquid and solid. For the initial equilibration period the thermostat is applied to both liquid and solid, but during the simulations to only the solid. The time step between computational iterations is 0.005 ps.

The two solid plates are constructed as rectangular, square-planar lattices having three atomic layers. The lattice parameter is $2^{1/6}\sigma_{SS}$ = 0.393 nm, i.e. the equilibrium distance between atoms interacting through the Lennard-Jones potential. The atoms are allowed to vibrate thermally around their initial positions according to a harmonic potential: $V_h(\vec{r}_i) = B\left|\vec{r}_i - \vec{r}_i^{\,0}\right|^2$. This provides a realistic solid surface that can exchange momentum with the liquid, yet is sufficiently rigid and impermeable. The gap *H* between the plates can be adjusted to study the effect of the size of the system on the results. Two gap widths have so far been investigated: 36.1 nm and 8.85 nm, designated 'large' and 'small'. For the small system, the plate dimensions are x = 69.6 nm by y = 12.3 nm, with periodic boundary conditions. Each contains 16 275 atoms. Plate dimensions for the large system are x = 59.6 nm by y = 7.6 nm, also with periodic boundary conditions, but containing 9 000 atoms. A larger x-dimension is needed to keep the liquid within the computational box. The smaller y-dimensions increase computational efficiency with no apparent loss of information.

The liquid is modeled as 8-atom chains, with adjacent atoms linked by a confining potential: $V_{conf}(r_{ij}) = Ar_{ij}^6$. This increases viscosity and restricts evaporation. The constant A is set to $\varepsilon_{ij}/\sigma_{ij}^6$. Standard methods [17] are used to determine the surface tension and shear viscosity of the liquid, γ_L = 2.49 ± 0.65 mN/m and η_L = 0.248 ± 0.004 mPa s, respectively. For the small system, 5 608 liquid molecules are used, with periodic boundary conditions in the y-direction. For the large system, the number of molecules was increased to 16 650.

At the start of each simulation the liquid index is equilibrated between the two plates for up to 1 500 time steps, as indicated by a contact angle that fluctuates about a constant value. To determine this angle, the positions of the front and back menisci are first located by a density calculation. Since there is no gravity, the menisci have constant curvature and the equilibrium contact angle θ^0 can be found by simply fitting an arc of a circle and measuring the tangent at the solid. A snapshot of the larger system with C_{A-B} = 0.5 shown in Figure 2(a).

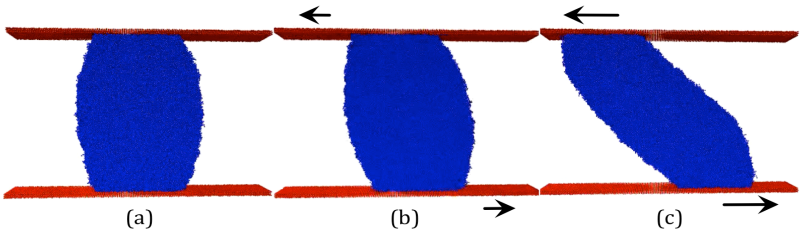

Fig. 2: Snapshots of the large system with a coupling C_{A-B} = 0.5: (a) at equilibrium, (b) and (c) at increasing plate speeds

To study forced wetting

we apply a velocity vector to the atoms in each of the plates to move them in opposite directions at a given speed and allow the system to evolve for 3×10^6 time steps. This is sufficient to achieve a steady state, as indicated by a steady dynamic contact angle θ_D. The angle is determined by a density calculation similar to that used for θ^0, but by fitting upper and lower parts of the meniscus with separate circular arcs. The observable speed range, though sufficient for our purpose, is limited by the stability of the liquid bridge, which ruptures at sufficiently high speeds. The change in shape of the liquid bridge as the speed is increased is illustrated in Figures 2(b) and 2(c).

To compute the details of the flow within the liquid bridge, we project the volume of the liquid onto the *x*-*y* plane, which we subdivide into a grid of small square cells. We compute the centre of mass of the molecules within each cell and then, after an interval of 10^4 time step, we repeat the process to calculate the net displacement. Finally we average the velocities over a fixed time interval. The size of the cells is chosen to ensure that each contains sufficient molecules to give reproducible results. In this way, we can measure the mean velocity of each cell to give lines of flux.

Results

The values of the equilibrium contact angles obtained at each coupling $C_{A\text{-}B}$ are listed in Table 1, together with those obtained previously from droplet spreading. There is excellent agreement, which confirms that we are working with the same system. In addition, the agreement between the angles found with the large and small systems shows that wetting is independent of the plate gap over the range studied.

Table 1: Equilibrium contact angles θ^0 and values of contact-line friction ζ for spreading drops and forced wetting

		Spreading drop		Forced wetting	
	$C_{A\text{-}B}$	θ^0 (deg)	ζ (mPa s)	θ^0 (deg)	ζ (mPa s)
Large system	0.4	134.8	0.121	135.8	0.0426
	0.5	121.3	0.235	120.9	0.0778
	0.6	105.8	0.348	106.9	0.147
	0.8	74.6	0.576	74.6	0.306
Small system	0.4	134.8	0.121	133.1	0.0263
	0.5	121.3	0.235	121.1	0.0557
	0.6	105.8	0.348	106.4	0.0839
	0.7	91.2	0.462	90.8	0.190
	0.8	74.6	0.576	75.8	0.356

Plots of $\gamma_{LV}(\cos\theta^0 - \cos\theta_D)$ versus U_{CL} for the large system are shown in Figure 3. Similar results were obtained with the small system. As can be seen, the data are essentially linear. Linear plots are expected as γ_L is small, which means that we can use eq. (2) to determine the contact-line friction ζ for each system from the slope. The resulting values, together with those for the small system and for the spreading drops are listed in Table 1. *It is immediately clear that the contact-line frictions for forced wetting are much smaller than those found for the spreading drops.* This difference is most pronounced at the lower couplings.

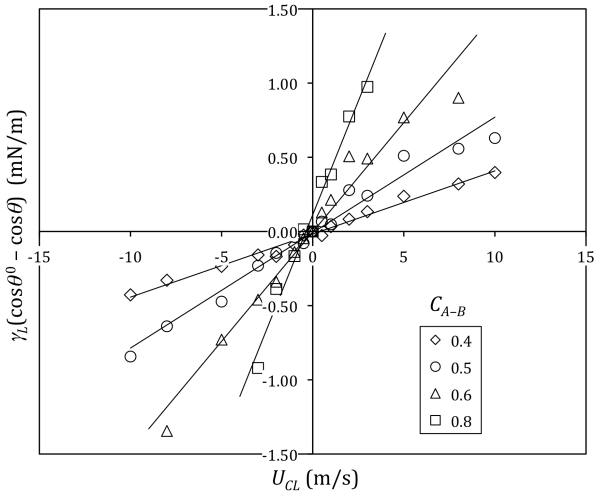

Fig. 3: Plots of the surface tension driving force $\gamma_{LV}(\cos\theta^0 - \cos\theta_D)$ versus contact-line velocity U_{CL} for the large system

In order to understand the cause of this effect, we studied the flow patterns within the liquid during the forced wetting simulations. Figure 4 (below) illustrates the patterns for both large and small systems with $C_{A\text{-}B}$ = 0.5 at 10 m/s. The arrows show the magnitude and direction of flow; the color-coding indicates the *x*-component of the velocity. In drop spreading the flow is mostly downwards towards the solid, with negligible tangential flow along the solid, except at the periphery [15]. In contrast, Figure 4 shows that in the forced wetting simulations there is a strong flow at the walls in the same direction as the plates.

However, the speed of the flow is significantly less than plate speed. In other words, there is slip between the liquid and the solid. Figure 5 shows the velocity of the first layer of liquid molecules U_1 plotted as a function of U_{Plate} for the four couplings explored with the large system. Evidently, U_1/U_{Plate}, decreases progressively with coupling. Hence, the slip speed $U_{Slip} = U_{Plate} - U_1$, which is in the direction of wetting, increases from 0.18 U_{plate} at $C_{A\text{-}B}$ = 0.8 to 0.5U_{Plate} at $C_{A\text{-}B}$ = 0.4. An increase in slip with θ^0 is in accord with our current understanding and similar levels of slip have been seen in other MD simulations [11,27].

Figure 4 also shows that there is a continuous 'tank-tread' flow around the boundary of the liquid with two inner eddies separated by a central stagnation point (more evident in the large system). This information allows us to estimate the shear stress driving slip in these confined environments as $\tau = \eta_L (du/dz) \sim \eta_L 2U_{Plate}/H$. The maximum speed observed with the small system was ~ 20 m/s, giving a shear rate approaching 5×10^9 s^{-1} and a shear stress at the wall of ~ 10^6 N/m^2. If we estimate the width of the contact-line region as the thickness of the liquid-vapor interface, which in our systems is about 2 nm, then since the out-of balance surface tension force acting at the contact line cannot exceed $2\gamma_L$ ~ 5 mN/m, the maximum shear stress this will produce is 2.5×10^6 N/m^2. Evidently, in the systems we have studied, the magnitudes of the forces involved in moving the contact line and those responsible for slip are very similar. Is it therefore surprising that we see a profound effect of flow on the dynamic contact angle and the apparent contact-line friction? The question we now address is how this might be rationalized within the context of the molecular-kinetic theory.

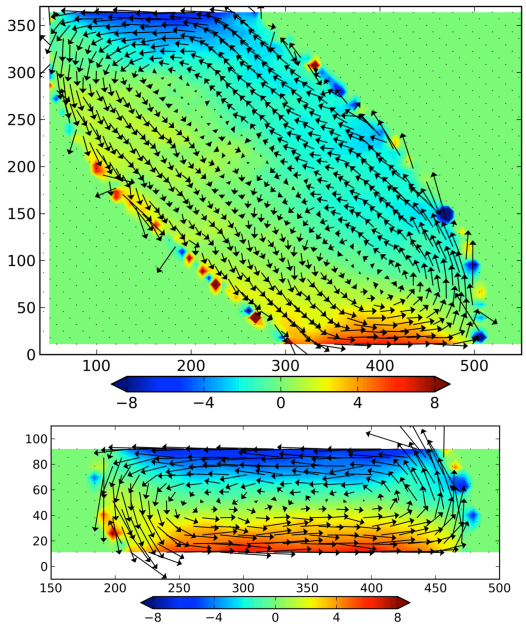

Fig. 4: Flow patterns at U_{CL} = 10 m/s and for large and small systems with $C_{A\text{-}B}$ = 0.5. The arrows and color-coding indicate the magnitude and direction of flow

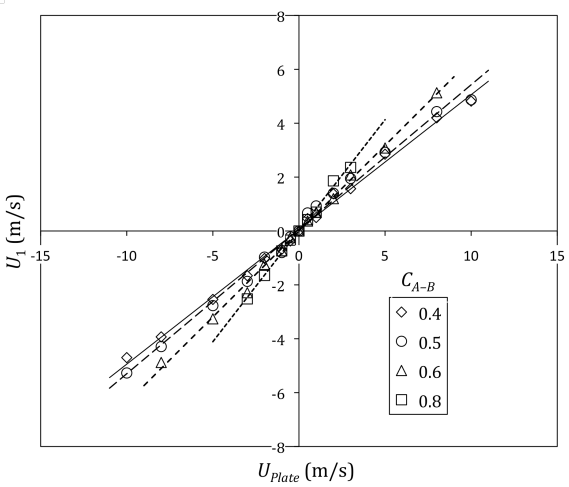

Fig. 5: Velocity of the first layer of liquid molecules U_1 plotted versus contact-line velocity U_{Plate} for the large system

Forced wetting, slip and the MKT

In the drop spreading studies, κ^0 was determined both from the dynamic contact angle data and directly from the simulations. Because there are very few molecules in the contact-line region, we made the measurements along the whole solid-liquid interface in order to improve the statistics. The resulting values obtained by the two methods were in good agreement, which implies that the statistical dynamics of the molecules at the contact line are the same as those at the general solid-liquid interface. That being the case, we can view contact-line friction and slip as simply different manifestations of the same underlying molecular process. However, while the force $\gamma_{LV}(\cos\theta^0 - \cos\theta_D)$ is responsible for moving the contact line at velocity U_{CL} against contact-line friction ζ, a force that can be estimated as

$\tau\delta = \eta_L\left(du/dz\right)\delta$ will be responsible for U_{Slip} against frictional forces at the general liquid-solid interface. Here, δ represents the size of the liquid molecules. If these ideas are correct and we assume a linear slip condition of the usual form

$$U_{Slip} = \tau/\beta \text{ or } U_{Slip} = \eta_L\left(du/dz\right)/\beta \tag{6}$$

where $\beta = \eta_L/l_{Slip}$ is the Navier slip coefficient and l_{Slip} is the slip length (i.e. the distance from the solid surface of the theoretical plane at which slip would be zero), then we can suppose that

$$\beta\delta = \zeta \text{ and } \tau\delta = \zeta U_{Slip} \tag{7}$$

However, while the force $\gamma_{LV}(\cos\theta^0 - \cos\theta_D)$ operates only at the contact line, the shear stress τ will act along the entire solid-liquid interface, *including the contact line*. Therefore, the total force at this location will be

$$f_{CL} = \gamma_L\left(\cos\theta^0 - \cos\theta_D\right) + \zeta U_{Slip} \tag{8}$$

Rewriting eq. (1) to include the additional term gives

$$U_{CL} = 2\kappa^0\lambda\sinh\left[\left(\gamma_L\left(\cos\theta^0 - \cos\theta_D\right) + \zeta U_{Slip}\right)/2nk_BT\right] \tag{9}$$

Thus, if U_{Slip} is significant, the extra driving force means that the increase in the dynamic contact angle required to overcome contact-line friction will be smaller. Hence, the overall velocity dependence of the contact angle will be reduced, as will the apparent contact-line friction. This can be seen most clearly if the argument of the sinh function in (9) is sufficiently small for U_{CL} to be linearly dependent on the driving force – as in the present simulations. Since both U_{CL} and U_{Slip} scale with $\kappa^0\lambda$, eq. (9) becomes

$$U_{CL} = U_{Slip} + \gamma\left(\cos\theta^0 - \cos\theta_D\right)/\zeta \tag{10}$$

Another way of viewing eq. (10) is to consider that the effective contact-line velocity is reduced to $U_{CL} - U_{Slip} = U_1$. This provides an immediate connection to hydrodynamic assist, i.e. higher coating speeds before θ_D approaches 180˚ and air is entrained. Furthermore, we can expect that the extent of hydrodynamic assist, which we might define as $U_{CL}/(U_{CL} - U_{Slip}) = U_{CL}/U_1$ will be given by ζ/ζ_F, where ζ_F is the apparent friction during forced wetting. In Figure 6, we have plotted the full dynamic contact angle curves for $C_{A\text{-}B} = 0.4$ and 0.8 for both drop spreading and forced wetting. These were calculated from eq. (1) using values of ζ from Table 1 and assuming that λ = 0.43 nm, as found in the drop spreading simulations [17]. Clearly, there is a very significant effect on the maximum speed of wetting, which roughly doubles for $C_{A\text{-}B} = 0.8$ and triples for $C_{A\text{-}B} = 0.4$ where slip is greater.

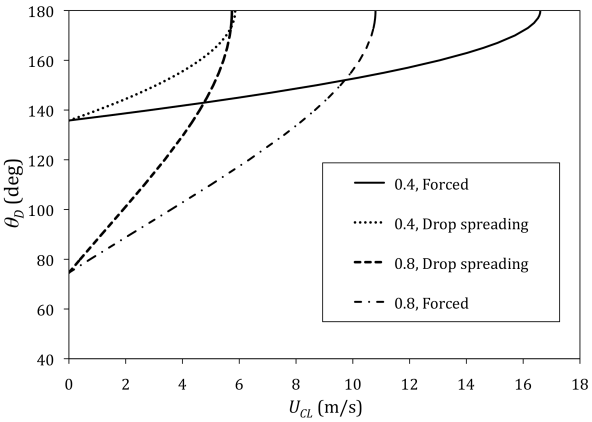

Fig. 6: Dynamic contact angle curves for $C_{A\text{-}B} = 0.4$ and 0.8 for both drop spreading and forced wetting

We can check how well these ideas hold up by using eq. (10) to predict U_1 for forced wetting from ζ for spreading drops. The results for all the large system are plotted in Figure 7, below. Overall, it would seem that eq. (10) underestimates U_1 by about 34%. However, given the fairly simple assumptions behind the slip model and the difficulties in measuring ζ and, in particular, U_1 with precision, the agreement is reasonably encouraging.

Finally, we note that by combining eqs. (4) and (7) we can derive an expression for the dependence of the slip length on the static contact angle

$$l_{Slip}/\delta = \left(\lambda/nv_L\right)\exp\left(-Wa^0/nk_BT\right) \tag{11}$$

A similar exponential relationship was derived more than 60 years ago by Tolstoi [28], though his equation contained the spreading coefficient $\gamma_{LV}(\cos\theta^0 - 1)$, which is zero or negative, rather than Wa^0, which is zero or positive, and therefore predicted much larger slip lengths.

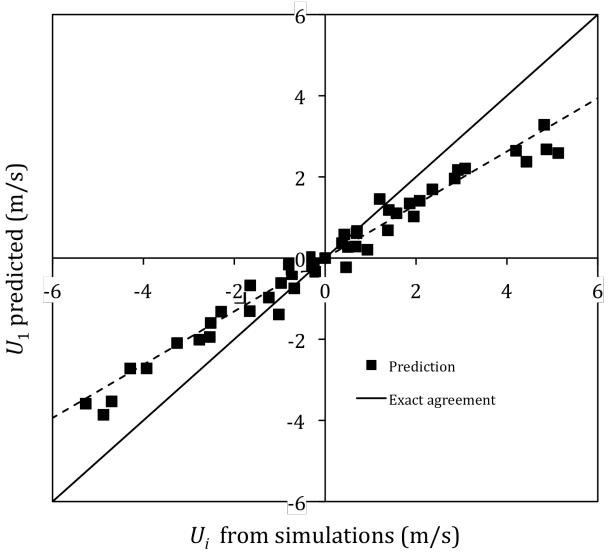

Fig. 7: Velocity of the first layer of molecules U_1 predicted by eq. (10) compared with that measured in the simulations for the large system

Summary and conclusions

We have employed large-scale molecular-dynamics simulations to model forced wetting with the same potentials, base parameters and methods previously used to model the spreading of liquid drops. This has enabled us to make a direct comparison between the two cases. By applying the molecular-kinetic theory to the observed velocity-dependence of the dynamic contact angle, we have been able to compare the contact-line frictions found for spontaneous and forced wetting. Significant differences have been found, with smaller apparent frictions for forced wetting. In addition, we have observed large slip velocities during forced wetting consistent with the intense shear fields generated in these small systems.

By extending the MKT to encompass slip at the general-sold liquid interface, we have been able to explain our results in a self-consistent way. We have shown that the shear stresses developed in these highly confined flows not only generate slip, but also provide an additional driving force at the contact line, comparable to the surface tension force, such that the apparent contact-line velocity is reduced to that of the first molecular layer in contact with the solid. This deceptively simple idea offers a possible explanation for the phenomenon known as hydrodynamic assist, whereby coating speeds may be increased substantially by manipulating and confining the flow in the vicinity of the moving contact line. While other factors, such as viscous bending of the liquid surface and the flow in the adjacent displaced phase, air, will undoubtedly play a role, we believe that our findings provide a potentially valuable insight into an ongoing industrial problem, namely, how to coat faster.

Acknowledgements

This research has been partially funded by the Interuniversity Attraction Poles Programme (IAP 7/38 MicroMAST) from the Belgian Science Policy Office, the Région Wallonne and the FNRS.

References

[1] Blake, T. D.; Clarke, A.; Ruschak, K. J. Hydrodynamic assist of dynamic wetting. *AIChE J.* **1994**, *40*, 229–242.

[2] Ngan, C, G.; Dussan V., E. B. On the nature of the dynamic contact angle: an experimental study. *J. Fluid Mech.* **1982**, *118*, 27–40.

[3] Kistler, S. F. Hydrodynamics of wetting. In *Wettability*; Berg, J. C., Ed.; Marcel Dekker: New York, 1993; pp 311–429.

[4] Vandre, E.; Carvalho, M. S.; Kumar, S. Delaying the onset of dynamic wetting failure through meniscus confinement. *J. Fluid Mech*. **2012**, *707*, 496–520.
[5] Blake, T. D. The physics of moving wetting lines. *J. Colloid Interface Sci*. **2006**, *299*, 1–13.
[6] Voinov, O. V. Hydrodynamics of wetting. *Fluid Dyn*. **1976**, *11*, 714–721.
[7] Cox, R. G. *J.* The dynamics of the spreading of liquids on a solid surface. *Fluid Mech.* **1986**, *16*, 169–194.
[8] Shikhmurzaev, Y. D. Moving contact lines in liquid/liquid/solid systems. *J. Fluid Mech*. **1997**, *334*, 211–249.
[9] Blake, T. D.; Haynes, J. M. Kinetics of liquid/liquid displacement. *J. Colloid. Interface Sci.* **1969**, *30*, 421–423.
[10] Blake, T. D. Dynamic contact angles and wetting kinetics. In *Wettability*; Berg, J. C., Ed.; Marcel Dekker: New York, 1993; pp 251–309.
[11] Lukyanov, A. V.; Likhtman, A. E. Relaxation of surface tension at the liquid–solid interfaces of Lennard-Jones liquids, *Langmuir* **2013**, *29*, 13996–1400.
[12] Duvivier, D.; Blake, T. D.; De Coninck, J. Towards a predictive theory of wetting dynamics. *Langmuir* **2013**, *29*, 10132–10140.
[13] Blake, T. D.; De. Coninck, J.; D'Ortona, U. Models of wetting: immiscible lattice Boltzmann automata versus molecular-kinetic theory. *Langmuir* **1995**, *11*, 4588–4592
[14] Koplik, J.; Banavar, J. R.; Willemsen, J. F. Molecular dynamics of fluid flow at solid surfaces. *Phys. Fluids A* **1989**, *1*, 781–794.
[15] de Ruijter, M. J.; Blake, T. D.; De Coninck, J. Dynamic wetting studied by molecular modeling simulations of droplet spreading. *Langmuir* **1999**, *15*, 7836–7847.
[16] Heine, D. R.; Grest, G. S.; Webb, E. B. III. Spreading dynamics of polymer nanodroplets. *Phys. Rev. E*. **2003**, *68*, 061603.
[17] Bertrand, E.; Blake, T. D.; De Coninck, J. Influence of solid-liquid interactions on dynamic wetting: a molecular dynamics study. *J. Phys. Condens. Matter* **2009**, *21,* 46124.
[18] Yue, P.; Feng, J. J. Can diffuse-interface models quantitatively describe moving contact lines? *Eur. Phys. J-Spec. Top.* **2011**, *197*, 37–46.
[19] Sibley, D. N.; Nold, A.; Sacca, N.; Kalliadasis, S. The contact line behaviour of solid-liquid-gas diffuse-interface models. *Phys. Fluids* **2013**, *25,* 092111.
[20] Ren, W.; Hu, D; E, W. Continuum models for the contact line problem. *Phys. Fluids* **2010**, *22*, 102103.
[21] Seveno, D.; Ogonowski, G.; De Coninck, J. Liquid coating of moving fiber at the nanoscale. *Langmuir* **2004**, *20*, 8385–8390.
[22] Blake, T. D.; Bracke, M.; Shikhmurzaev, Y. D. Experimental evidence of nonlocal hydrodynamic influence on the dynamic contact angle. *Phys. Fluids* **1999**, *11*, 1995–2007.
[23] Blake, T. D.; Dobson, R. A.; Ruschak, K. J. Wetting at high capillary numbers. *J. Colloid Interface Sci*. **2004**, *279*, 198–205.
[24] Clarke, A.; Stattersfield, E. Direct evidence supporting nonlocal hydrodynamic influence on the dynamic contact angle. *Phys. Fluids* **2006**, *18*, 048109.
[25] Blake, T. D.; De Coninck, J. The influence of solid–liquid interactions on dynamic wetting. *Adv. Colloid Interface Sci.* **2002**, *96*, 21–36.
[26] Li, H.; Sedev, R.; Ralston, J.; Dynamic wetting of a fluoropolymer surface by ionic liquids. *Phys. Chem. Chem. Phys*. **2011**, *13*, 3952–3959.
[27] Lauga, E.; Brenner, M. P.; Stone, H. A. Microfluidics: the no-slip boundary condition. In *Springer Handbook of Experimental Fluid Mechanics*; Foss, J.; Tropea, C.; Yarin, A., Eds.; Springer: Berlin, 2007; pp 1219–1240.
[28] Blake, T. D. Slip between a liquid and a solid: D. M. Tolstoi's (1952) theory reconsidered. *Colloids Surfaces* **1990**, *47*, 135–145.